

國立臺灣大學理學院物理學研究所



碩士論文

Department of Physics

College of Science

National Taiwan University

Master Thesis

透過螢光共振能量轉移實現

高亮度混合磷化銦量子點發光二極體

Highly Luminescent Emission of Mixed InP Quantum Dot

Light-Emitting Diodes through Förster Resonance Energy

Transfer

呂道峰

Tao-Feng Lu

指導教授：陳永芳 博士

Advisor: Yang-Fang Chen, Ph.D.

中華民國 112 年 7 月

July, 2023

國立臺灣大學碩士學位論文
口試委員會審定書
MASTER'S THESIS ACCEPTANCE CERTIFICATE
NATIONAL TAIWAN UNIVERSITY

透過螢光共振能量轉移實現
高亮度混合磷化銦量子點發光二極體

Highly Luminescent Emission of Mixed InP Quantum Dot Light-
Emitting Diodes through Förster Resonance Energy Transfer

本論文係__呂道峰__(姓名)__R10222065__(學號)在國立臺灣大
學__物理學研究所__(系/所/學位學程)完成之碩士學位論文，於民國
112年7月19日承下列考試委員審查通過及口試及格，特此證明。

The undersigned, appointed by the Department / Institute of _____ physics
on 19 (date) July (month) 2023 (year) have examined a Master's thesis entitled above presented
by Tao-Feng Lu (name) R10222065 (student ID) candidate and hereby certify that it is
worthy of acceptance.

口試委員 Oral examination committee:

沈永芳
(指導教授 Advisor)

沈志壽

許易堃

系主任/所長 Director:



致謝



時間飛逝，兩年的碩士生涯即將告一段落。在實驗室的這段期間，真的受到了許多人的幫助，我打從心底非常感激。是因為有大家的幫助，我才能克服兩年來的所有挑戰，這篇論文也才能順利誕生。

謝謝陳永芳老師兩年來的指導。老師給了我很多研究方向上的建議，就連我犯錯或迷惘時，老師的指教也是充滿耐心與包容，讓我能在研究中前往正確的方向。感謝許芳琪、沈志霖教授，以及謝馬利歐教授，在口試以及 meeting 時的傾聽與反饋。教授們珍貴的意見使我成長不少。謝謝夏玉學姐，學姐帶領我進入了研究領域，手把手教導我許多的實驗技巧與方法。學姐總是在我面臨問題時，給予我最大、最即時的幫助。學姐嚴謹的態度也深深影響了我。謝謝家宇學長，學長不僅教了我一些儀器的操作，每次有事情求助於學長時，學長總會立即放下手邊工作來協助我。謝謝冠璋學長常常主動關心我的實驗狀況，並給予我很實用的建議。謝謝育銓學長、育傑學長、承甫學長、仲涵學姐、序彥學長幫我解決許多實驗上遇到的問題。謝謝昕恩給了我很多重要的資料和資訊，甚至主動幫我跑了不少麻煩程序，也謝謝政勳、郁軒、嘉尉、念修，感謝大家的意見交流與不吝嗇的幫助。謝謝實驗室的大家。最後也感謝家人及朋友的默默支持。

這兩年面對到不少挑戰與挫折，但遇到的這些人、事、物，讓我覺得自己很幸運。向所有幫助過我的人致上最深的謝意。

中文摘要

近年來，由於環保、無毒的特性，磷化銦量子點的發展及應用逐漸受到矚目。

本論文中，我們探討了 534 nm、607 nm 磷化銦量子點之間的螢光共振能量轉移特性，使得量子點發光強度和載子生命週期有所提升。此外，我們成功地利用溶劑製程製造出以混合磷化銦量子點為主動發光層的發光二極體，其最大電流效率可達 28.9 cd A^{-1} ，而外部電子效率可達 10.6%，相比於其他相似結構但沒有混和量子點發光層的已發表報告，效率大約可提升至兩倍。我們設計的磷化銦量子點發光二極體元件具有簡單易製作的結構，提出的機制和製程方法很也很容易複製並應用在其他材料，使其在光電技術的開發中具有極高的實用性和潛力。

關鍵字：磷化銦、無鎘量子點、量子點發光二極體、螢光共振能量轉移

Abstract



In recent years, there has been a growing interest in the development and application of indium phosphide (InP) quantum dots (QDs) due to their eco-friendly and non-toxic characteristics. We investigated the Förster resonance energy transfer (FRET) between 534 nm and 607 nm InP QDs to enhance the emission and carrier lifetime from 607 nm InP QDs. We further fabricated mixed InP quantum dot light-emitting diodes (QD-LEDs) using a solution-processed fabrication method. FRET was employed in the InP light emitting layer by utilizing a mixture of 607 nm and 534 nm QDs to enhance the emission efficiency. The best-performing mixed InP QD-LED device achieved a maximum current efficiency of 28.9 cd A^{-1} and an external quantum efficiency (EQE) of 10.6%, which is about two times better than those achieved by the pure QD device and other published reports with similar structures without QD mixture. The mechanisms presented here can be further replicated and applied in many other material systems, and the simple and easily-fabricated layer structure of the QD-LED devices makes them highly practical and promising for the development of efficient optoelectronic technology.

KEYWORDS: InP, Cd-free quantum dots, quantum dots LED, FRET

Contents



致謝.....	i
中文摘要.....	ii
Abstract.....	iii
Contents	iv
List of Figures	vi
Chapter 1.....	1
Introduction.....	1
Chapter 2	3
Theoretical Background.....	3
2.1 Photoluminescence (PL)	3
2.2 Time-Resolved Photoluminescence (TRPL)	3
2.3 Electroluminescence (EL).....	4
2.4 Förster resonance energy transfer (FRET).....	5
2.5 External Quantum Efficiency (EQE)	7
Chapter 3	8
Experimental Details	8
3.1 Equipment.....	8



3.1.1 SEM	8
3.1.2 PL apparatus.....	9
3.1.3 EL apparatus	9
3.2 Material preparation.....	10
3.2.1 Synthesis of ZnO nanoparticle.....	10
3.3 Device Fabrication	10
3.4 Experiment.....	11
Chapter 4	13
Results and Discussion.....	13
4.1 Device struture	13
4.2 Properties of the QDs mixture layer	14
4.3 Performance of the quantum dot light-emitting diode device	21
Chapter 5	31
Conclusion	31
Reference	32

List of Figures



Figure 2.1 Illustration of electroluminescence process in inorganic and organic

LEDs^[19]. 5

Figure 2.2 Basic principles of FRET. (A) Jablonski diagram illustrating

excitation and emission of the donor and FRET between the donor and

acceptor, resulting in acceptor emission. (B) Dependence of FRET efficiency

on the distance between donor and acceptor molecules. Förster radius R_0 is

the distance at which half of the energy of the excited donor is transferred

by FRET^[31]. 6

Figure 3.1 Illustration of photoluminescence setup^[34]. 9

Figure 4.1 (a) Schematic of the mixed InP QD-LED device structure (b) Top

scanning electron microscopy image (SEM) and (c) Cross-sectional SEM

image of the mixed InP QDs layer spin-coated on silicon.17

Figure 4.2 Photoluminescence spectra of mixed InP QDs with various ratios of

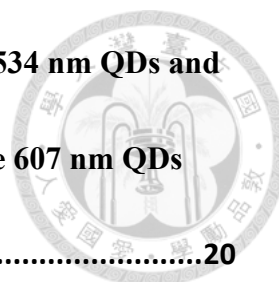
534 nm QDs and 607 nm QDs.18

Figure 4.3 (a) Absorption and emission spectra of InP 607 nm QDs and emission

spectrum of InP 534 nm QDs (b) Photoluminescence spectra of pure QDs

and a 1:3 mixture of 534/607 nm QDs.19

Figure 4.4 Time-resolved photoluminescence spectra of pure QDs and a 1:3



mixture of InP 534/607 nm QDs. (a) TRPL spectra of pure 534 nm QDs and mixed QDs, monitored at 534 nm. (b) TRPL spectra of pure 607 nm QDs and mixed QDs, monitored at 607 nm.20

Figure 4.5 Schematic energy band diagram of the mixed InP QD-LED device...25

Figure 4.6 Current-voltage characteristic of the mixed InP device. The inset shows the real photo of the red-light emission from the mixed InP QD-LED device.....26

Figure 4.7 (a) EL spectra of the mixed InP QD-LED device at various levels of current injection. Inset is a zoomed-in EL spectra at current injection levels of 5.0, 7.5, and 10.0 mA. (b) A comparison between the PL spectrum of the QDs layer and the EL spectrum of the mixed InP QD-LED device under a current injection of 25 mA.27

Figure 4.8 (a) Peak intensities of the red and green spectra as a function of different current injections (b) Ratio between the red and green peak intensities as a function of different current injections. The dashed line represents the ratio observed in the photoluminescence spectrum.28

Figure 4.9 Luminous current efficiency and EQE of the mixed InP QD-LED device at different current injections.29

Table 4. 1 Performances of the previously reported red InP QD-LEDs,30



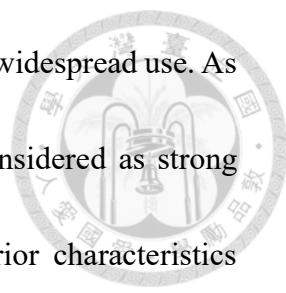
Chapter 1

Introduction



In recent years, quantum-dot light-emitting diodes (QD-LEDs) have gained significant attention due to the unique advantages of quantum dots (QDs). QDs are semiconducting nanocrystals with diameters below 20 nm^[1]. Their optical properties, such as emission wavelength, are dependent on the size and shape of the QDs. Therefore, by precisely controlling the size of QDs, we can achieve specific emission colors^[2]. This size-tuned bandgap is a result of the quantum confinement effect, allowing for a wide range of emission spectra from ultraviolet to visible to infrared^[1]. QD-LEDs offer several advantages, such as precise color control, high fluorescent efficiency, and a narrow emission bandwidth^[3]. These advantages make QD-LEDs promising for applications in displays, lighting, and optoelectronic devices^[4-5].

In particular, solution-processed QD-LEDs are considered a promising technology due to their simplicity and cost-effectiveness in fabrication^[6-8]. They have potential application for large area displays and flexible devices. While there have been remarkable achievements in the material development of QD-LED devices, the most remarkable performances have been achieved using Cd-based QD materials such as CdSe and CdS^[9-10]. However, the potential toxicity and environmental contamination



associated with Cd-based QDs have raised concerns regarding their widespread use. As a result, cadmium free indium phosphide (InP) QD have been considered as strong contenders due to their non-toxic elements. InP QDs have superior characteristics compared to Cd-based QDs, such as a larger bulk bandgap and Bohr radius, resulting in wide spectral tunability ranging from deep blue to near infrared^[11-13]. Though InP quantum dots may exhibit less luminescent efficiency and have a relatively shorter device lifetime compared to CdSe-QD-LEDs, their innocuity nature still makes them an attractive alternative^[14-18]. Therefore, improving the light-emitting efficiency and expanding the range of applications for InP QDs devices has become a prominent goal. Researchers are actively working towards enhancing the performance of InP devices to achieve higher levels of light emission efficiency.

In this thesis, we successfully demonstrated all solution-processed mixed InP QD-LEDs with high efficiency and performance. Additionally, we investigated and implemented Förster resonance energy transfer (FRET) in the InP QDs layer to enhance the luminous efficiency and of mixed InP QD-LEDs. Our findings provide valuable insights into the design and optimization of solution-processed InP QD-LEDs, opening up new possibilities for highly efficient and versatile light-emitting devices.

Chapter 2

Theoretical Background



2.1 Photoluminescence (PL)

Photoluminescence (PL) refers to the emission of light from a material after illuminated. When a material absorbs photons with energy larger than its bandgap, electrons within the material will be excited to higher energy levels. When these excited electrons return to their ground state, they release energy in the form of light. This phenomenon is commonly observed in various materials such as semiconductors, quantum dots, and organic molecules. PL spectroscopy provides us with a non-contact, nondestructive method for analyzing the emission behavior of materials. Therefore, PL is a widely used technique in materials science, physics, and chemistry.

2.2 Time-Resolved Photoluminescence (TRPL)

Time-resolved photoluminescence (TRPL) is a technique used to study the temporal dynamics of PL emission from a material. In a TRPL experiment, a pulsed laser is used to excite the electrons in the material to a higher energy level. Once excited, the electrons in the material relax back to their ground state, emitting light in the process. TRPL provides information about the timescale of the emission process. By measuring

and analyzing the decay of the emitted light over time, we can get some information about recombination mechanisms, such as lifetime.



2.3 Electroluminescence (EL)

Electroluminescence (EL) is an optical phenomenon that leads to emission from the material. For the material, usually semiconductor, when a voltage is applied or there is current flow, electrons are injected into the conduction band from the cathode, while holes are injected into the valence band from the anode. The holes and electrons then recombine and emit photons. This phenomenon is called EL. This phenomenon is commonly observed in light-emitting devices.

For an organic light-emitting diode (OLED) or a solution-processed QD-LED, the device structure typically consists of several layers. These include a hole transport layer and an electron transport layer, with an active layer sandwiched between them. When a voltage is applied between the cathode and anode of the device, electrons and holes are injected into the active layer. The active layer is where holes and electrons recombine and generate photons.

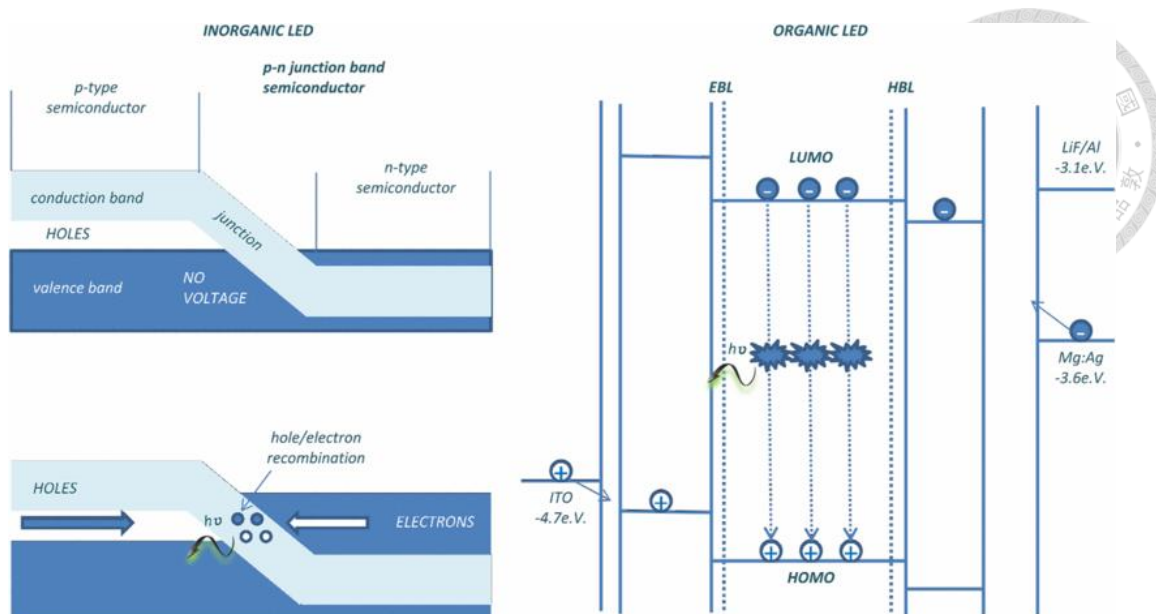


Figure 2.1 Illustration of electroluminescence process in inorganic and organic LEDs^[19].

2.4 Förster resonance energy transfer (FRET)

Förster resonance energy transfer (FRET) is defined as a nonradiative energy transfer process from an excited donor to an acceptor through dipole-dipole interactions, which enhances the emission of the acceptor. FRET has been widely studied and has shown its potential value in various applications, including biosensing, solar cells, and protein conformation studies^[20-22]. The efficiency of FRET depends on several factors, including the distance between the donor and acceptor molecules, their spectral overlap, and the orientation of their transition dipole moments^[20, 23-24]. The efficiency of FRET decreases as the distance between the donor and acceptor increases, which can be quantitatively described by the equation^[25-26]:

$$E = \frac{1}{1 + \left(\frac{R}{R_0}\right)^6}$$



where E is the FRET efficiency, R is the distance between the donor and acceptor, and R_0 is the Förster radius. FRET only occurs when they are within a range of a few nanometers, typically 1 to 10 nm^[27-30]. Overlap between PL spectrum of the donor and the absorption spectrum of the acceptor is also crucial. Therefore, selecting appropriate donor and acceptor materials is essential for efficient FRET. When FRET occurs, it leads to reduction of donor's lifetime and increasing of acceptor's lifetime. Therefore, by measuring TRPL of a sample containing donor and acceptor molecules, we can observe changes in the fluorescence lifetimes that provide evidence of FRET.

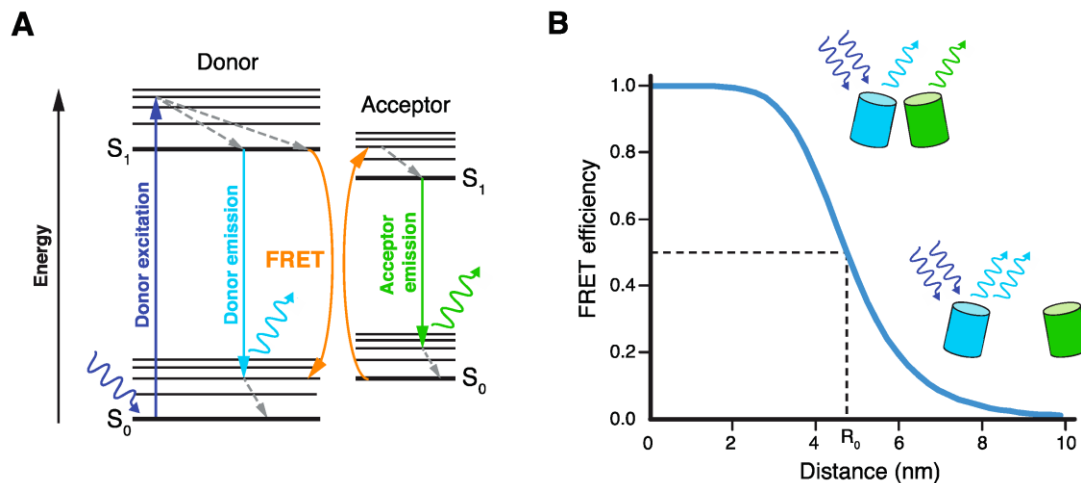


Figure 2.2 Basic principles of FRET. (A) Jablonski diagram illustrating excitation and emission of the donor and FRET between the donor and acceptor, resulting in acceptor emission. (B) Dependence of FRET efficiency on the distance between donor and acceptor molecules. Förster radius R_0 is the distance at which half of the energy of the excited donor is transferred by FRET^[31].



2.5 External Quantum Efficiency (EQE)

External quantum efficiency (EQE) of an LED is defined as the ratio of emitted photons over injected charges. A higher EQE value indicates a higher efficiency of photon emission for a given number of injected electrons. EQE value η_{ext} can be calculated by the equation^[32-33]:

$$\eta_{ext} = \frac{N_p}{N_e} = \frac{P/h\nu_{avg}}{I/e} = \frac{P / \left(\frac{hc}{\lambda}\right)_{avg}}{I/e} = \frac{P}{1240 \times I \times (1/\lambda)_{avg}}$$

Where N_p is the emitted photon number per second, N_e is the injected electron number per second, P is the emission power in watts, ν_{avg} is the average emission light frequency, λ is the light emission wavelength (in nanometer for the last equation), and I is the injected current in amperes. P represents the total emission energy per second, dividing it by $\left(\frac{hc}{\lambda}\right)_{avg}$, an average energy of each emitted photon, we can get the number of photons emitted per second. And then divided by I/e , the number of injected electrons per second, we can get the EQE of the device.

Chapter 3

Experimental Details



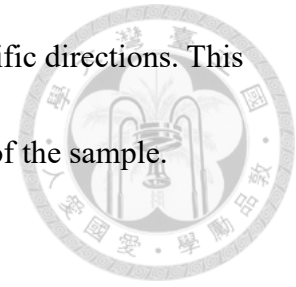
3.1 Equipment

3.1.1 SEM

SEM (Scanning Electron Microscope) is a type of electron microscope. SEM uses a focused electron beam to generate images by detecting the electrons reflected from or scattered near the surface of the sample. The resolution of a microscope is influenced by the wavelength of the imaging beam, as a result of diffraction. Compared to optical microscopes, SEM offers higher resolution capabilities due to the much smaller wavelength of electrons compared to light.

The components of SEM include an electron source, lenses, a scanning coil, a sample chamber, and detectors. Electron source is made of tungsten filament, which can be heated and produced electrons. Electrons then accelerate and inject into the system by applying a high voltage. Lenses are used to focus the electron beam, while scanning coil is used to adjust x-y axis of electron beam on the surface of sample. Sample chamber is where the sample is placed and is evacuated during the measurement process. When the electron beam hits and interacts with the sample, secondary electrons and backscattered electrons are ejected from the sample. By using detectors, we can

measure the energy loss or intensity of the ejected electrons in specific directions. This information allows us to obtain details about the internal structure of the sample.



3.1.2 PL apparatus

In our study, PL experiment setup including a laser, optical lens and mirror system, monochromator and detector. The laser is provided by a 374 nm pulsed laser as excitation source, the optical lens and mirror system is used for directing and focusing the light, while the monochromator is used for selecting specific wavelengths to transmit to the detector.

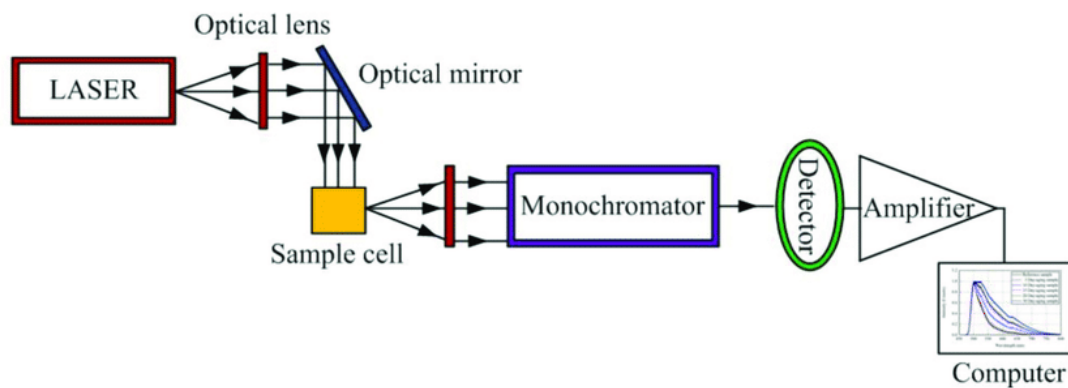


Figure 3.1 Illustration of photoluminescence setup^[34].

3.1.3 EL apparatus

For the EL measurement, the experimental setup includes a power supply connected to the sample to provide the necessary voltage or current injection for the sample to emit light. Additionally, a spectrometer and a CCD (charge-coupled device)

are included in the setup to measure and analyze the emission spectrum.



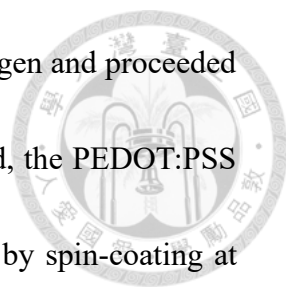
3.2 Material preparation

3.2.1 Synthesis of ZnO nanoparticle

440 mg of zinc acetate (CH_3COOZn) was dissolved in 20 mL of 99.5% ethanol by stirring for 5 minutes, followed by ultrasonic bath for 10 minutes. Then, 116 mg of lithium hydroxide (LiOH) was added to the solution and subjected to an ultrasonic bath for 30 minutes. Then, 400 μL of deionized water was added to the solution, and it was heated in a hot water bath at 60 °C for 30 minutes. During this time, the ZnO nanoparticles started to synthesize. Once the solution was cooled down by cold water, it was purified by centrifugation. The solution was centrifuged twice, first at 3000 rpm for 2 minutes, and then at 5000 rpm for another 2 minutes. This process was done to remove any impurities and acetate salt and ensure that the ZnO nanoparticles were of high quality. At last, ZnO was dissolved in isopropanol to a concentration of 15 mg/mL, and ethanolamine (6 $\mu\text{L}/\text{mL}$) was added to the solution, followed by an ultrasonic bath for 120 minutes.

3.3 Device Fabrication

First, ITO-coated glass substrates were cleaned using an ultrasonic cleaning process. The substrates were cleaned sequentially with soap water, deionized water,

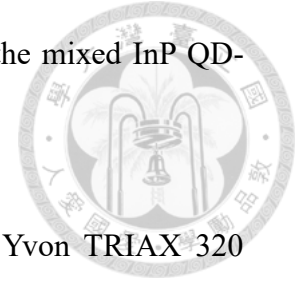


acetone, and ethanol. The substrates were then blown dry with nitrogen and proceeded to the oxygen-plasma cleaning procedure for 10 minutes. Afterward, the PEDOT:PSS solution was deposited onto the clean ITO-coated glass substrates by spin-coating at 3000 rpm for 60 seconds, followed by baking at 120 °C for 10 minutes. The PVK solution (3 mg/mL in toluene) was then spin-coated at 3000 rpm for 60 seconds and baked at 150 °C for 30 minutes. The InP QDs (Unique Materials HCC-0049 and HTY-0037) mixture solution (15 mg/mL in toluene) with different ratio of 534 nm and 607 nm QDs was spin-coated at 700 rpm for 120 seconds. The synthesized ZnO nanoparticles solution (15 mg/mL in isopropanol) was spin-coated at 800 rpm for 60 seconds. Finally, Ag electrodes were deposited on the top of the device to 100 nm using a thermal evaporation system under a high vacuum of 6×10^{-4} Pa.

3.4 Experiment

This study investigates the FRET of the mixture of InP QDs consisting of green QDs with a 534 nm emission as the energy donors and red QDs with a 607 nm emission wavelength as the energy acceptors. We prepared a QDs mixture solution with a specific weight ratio at 534 and 607 nm QDs of concentration 15 mg/mL in toluene, which was then spin-coated onto a silicon wafer. We conducted SEM and PL measurements on the coated sample. We further demonstrated a mixed InP QD-LED device that exhibits enhanced emission as a result of FRET and the reduction of reabsorption effect

occurring in the active layer. The detailed fabrication method of the mixed InP QD-LED device is presented in the section 3.3.



PL and TRPL spectra were acquired using a Horiba Jobin Yvon TRIAX 320 spectrometer, with excitation provided by a 374 nm pulsed laser. Absorption measurements were performed using a PerkinElmer LAMBDA 750 ultraviolet/visible/near-infrared spectrophotometer. The current-voltage characteristic was recorded by a Keithley 2400 electrometer as the power source, controlled by KickStart software. EL spectra were measured using a high-resolution Jobin Yvon iHR550 spectrometer equipped with gratings of 300 grooves/mm. The images for cross sections of the samples were acquired by a JEOL JSM-6500F field emission scanning electron microscope.

Chapter 4

Results and Discussion



4.1 Device structure

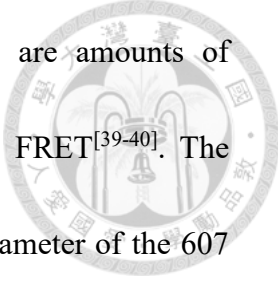
The QD-LED device was designed as a multilayer structure, including organic nanoparticles and non-organic quantum dots. The device was fabricated on an indium tin oxide (ITO) substrate using a solution-processed approach, consisting of 4 layers. The transparent electrode was made of ITO while the hole transport layer comprised PEDOT:PSS (poly(3,4-ethylenedioxythiophene): polystyrene sulfonate) and PVK (poly(9-vinylcarbazole)). The active layer consisted of a mixture of 534 nm and 607 nm InP QDs in a ratio of 1:3, and the electron transport layer included ZnO nanoparticles. Finally, an Ag film with a thickness of 100 nm was deposited as the cathode. **Figure 4.1a** shows the schematic diagram of the device structure. Bilayer structure of PEDOT:PSS/PVK is a common choice for hole transport layer. PEDOT:PSS helps to reduce the surface roughness of ITO while providing excellent conductivity, whereas PVK offers the advantage of electron-blocking capability^[35-36]. ZnO is widely used as an electron transport layer due to its suitable energy band alignment, simple solution processibility, and excellent electron transport properties^{[37-}

38]

4.2 Properties of the QDs mixture layer

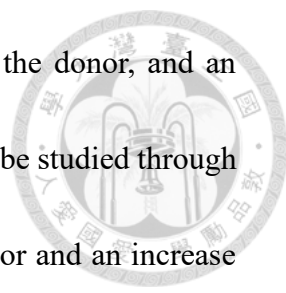


Figure 4.1b shows the scanning electron microscopy (SEM) top-view image of a mixed InP QDs film on a silicon substrate. The film consists of a mixture of 534 nm and 607 nm QDs with a ratio of 1:3, which were spin-coated onto the substrate. **Figure 4.1c** displays the cross-sectional SEM image of the mixed InP QDs film. The SEM images confirm that the surface of the film is flat and uniform, and the approximate thickness of the film is 87 nm. **Figure 4.2** shows the photoluminescence (PL) spectra of mixed InP QDs with different solution weight ratios of 534 nm QDs and 607 nm QDs ranging from 1:1 to 1:5. As the proportion of 607 nm QDs in the mixture increases, the color of the PL shifts from orange to red. For the PL spectra, the intensity of the green band gradually decreases. The intensity of the red band increases as the ratio progresses from 1:1 to 1:3. However, when the ratio reaches 1:4, there is no further increase observed in the intensity of the red band. The decrease in green band luminescence and increase in red band emission are not only caused by the reduction of 534 nm QDs or the increase in 607 nm QDs. FRET between the two types of QDs also contributes to the decrease in green band luminescence and enhancement of red band luminescence. From the growth and decline trend of spectra, a weight ratio of 1:3 between 534 nm and 607 nm QDs is determined to be the optimal ratio for achieving efficient FRET. To maximize the energy transfer efficiency, it is crucial to have a



balanced number of donor and acceptor QDs. Otherwise, there are amounts of uncoupled acceptor or donor molecules that do not contribute to FRET^[39-40]. The diameter of the 534 nm QDs was approximately 7 nm, while the diameter of the 607 nm QDs was around 10 nm. As a result, the size ratio between the 534 nm QDs and 607 nm QDs was approximately 1:3. This size ratio helps to explain the higher energy transfer efficiency observed in the mixture with a 1:3 ratio compared to other ratios.

In **Figure 4.3a**, the normalized absorption and emission spectra of InP 534 nm QDs and the emission spectra of InP 607 nm QDs are presented. The 607 nm QDs exhibit an emission band at 607 nm, while 534 nm QDs demonstrate a broad absorption range from 450nm to 600nm. There is a significant spectral overlap between the absorption spectrum of the 607 nm QDs and the emission spectrum of the 534 nm QDs. This spectral overlap suggests the potential occurrence of FRET from the 534 nm QDs to the 607 nm QDs upon combining these two materials. The PL spectra of the pure and mixture InP QDs are presented in **Figure 4.3b**. After combining 607 nm and 534 nm QDs, the intensity peak of the red band increases, while the intensity peak of the green band decreases. The decrease in the intensity of the green band indicates strong evidence of energy transfer from the 534 nm to the 607 nm QDs within the mixture^[22, 41-42]. Note that the peak intensity of the 607 nm red emission is about two times larger than that of the pure 607 nm QDs without mixture. When FRET occurs, energy transfer



results in a decrease in the fluorescence intensity and lifetime of the donor, and an increase in the emission of the acceptor. The underlying process can be studied through TRPL experiments, where a reduction in the PL lifetime of the donor and an increase in the acceptor's PL lifetime can be observed^[20, 22, 43]. In **Figure 4.4a**, we investigate the TRPL spectra of pure 534 nm QDs and mixed QDs, monitored at 534 nm which corresponds the peak wavelength of pure 534 nm QDs. **Figure 4.4b** displays the TRPL spectra of pure 607 nm QDs and mixed QDs, monitored at 607 nm, which corresponds the peak wavelength of pure 607 nm QDs. The lifetime τ can be obtained by fitting the data with the exponential decay function $I(t) = I_0 e^{-t/\tau}$, and then extracting the lifetime parameter τ . Based on the TRPL spectra, we observed a decrease in the lifetime of 534 nm QDs from 9.38 ns to 6.37 ns as they were mixed with 607 nm QDs. In contrast, the lifetime of 607 nm QDs increased from 8.83 ns to 12.19 ns after mixing with 534 nm QDs. These results support the principle behind FRET process, which shorten the donor's lifetime and longer the acceptor's lifetime. Moreover, the FRET efficiency (E) can be calculated using the equation^[44-45]:

$$E = 1 - \frac{\tau_{DA}}{\tau_D},$$

where τ_{DA} and τ_D are the lifetime of the donor in the presence or absence of the acceptor, respectively. For our sample, the FRET efficiency from 534 nm QDs to 607 nm QDs is 32%.

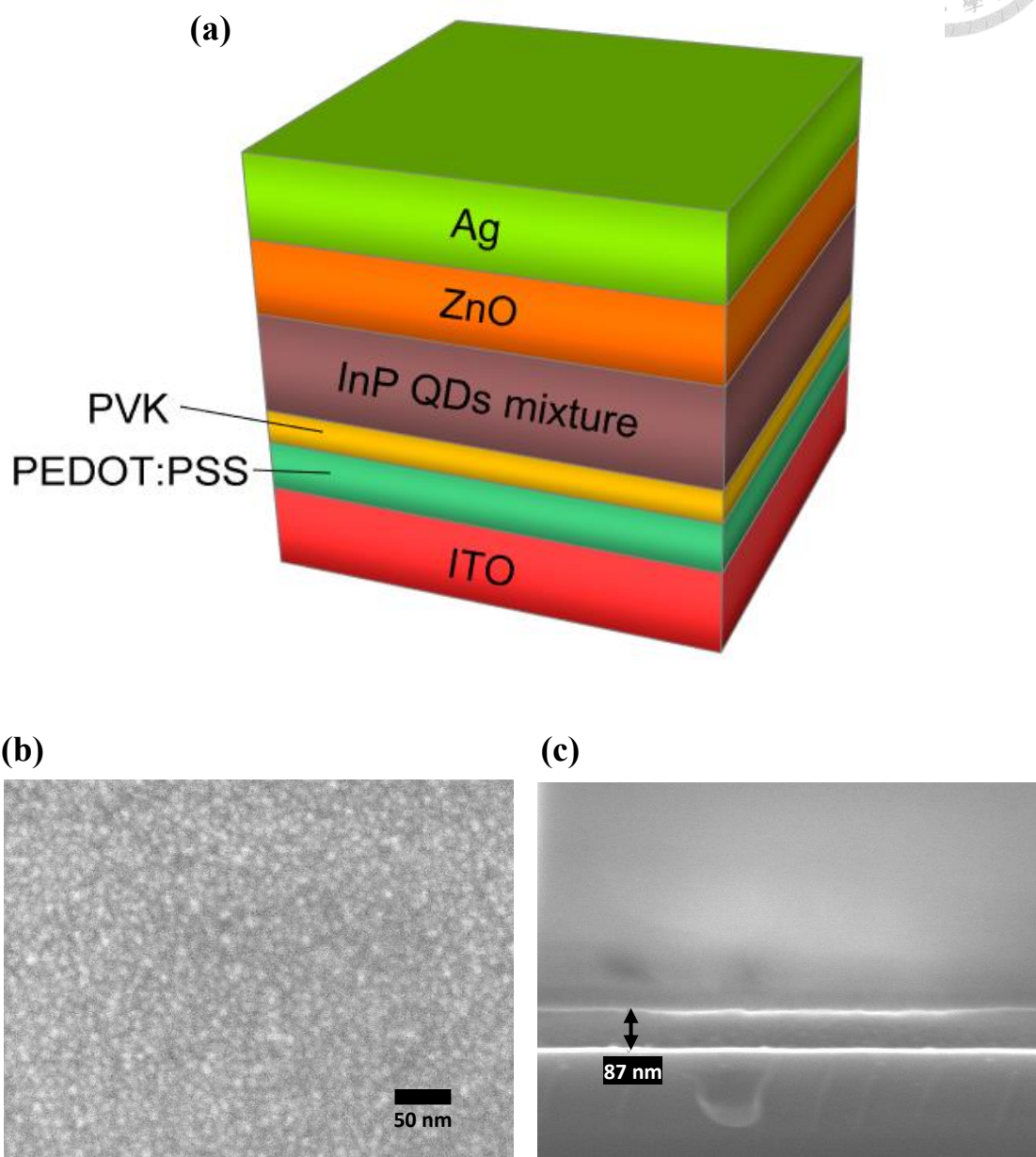


Figure 4.1 (a) Schematic of the mixed InP QD-LED device structure (b) Top scanning electron microscopy image (SEM) and (c) Cross-sectional SEM image of the mixed InP QDs layer spin-coated on silicon.

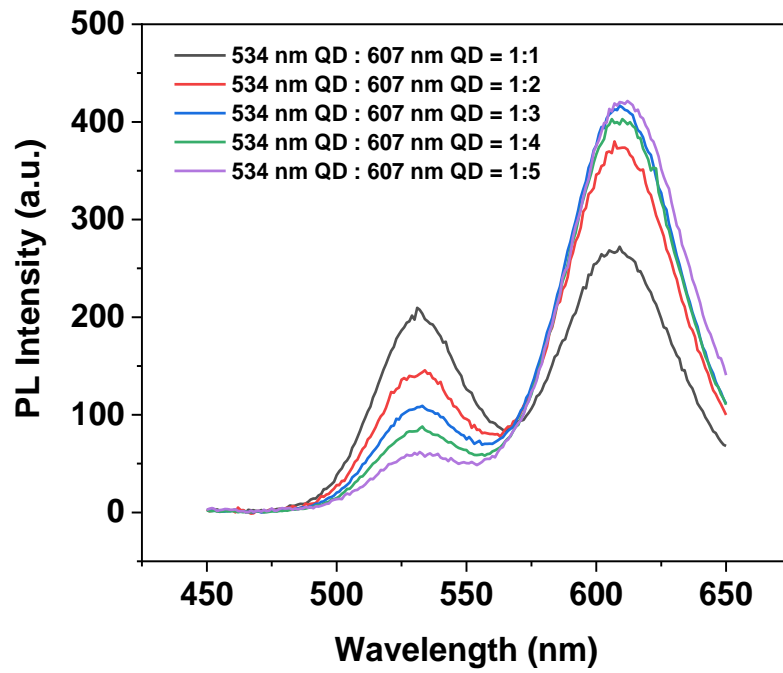


Figure 4.2 Photoluminescence spectra of mixed InP QDs with various ratios of 534 nm QDs and 607 nm QDs.

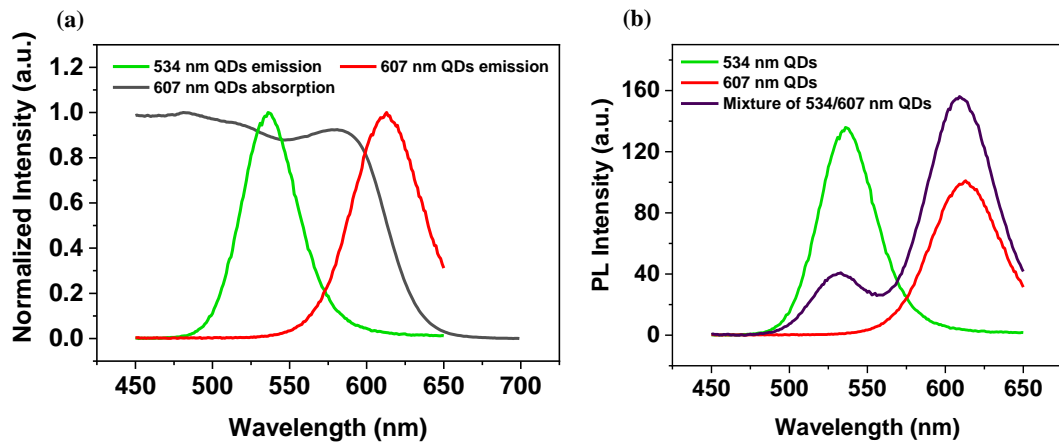


Figure 4.3 (a) Absorption and emission spectra of InP 607 nm QDs and emission spectrum of InP 534 nm QDs (b) Photoluminescence spectra of pure QDs and a 1:3 mixture of 534/607 nm QDs.

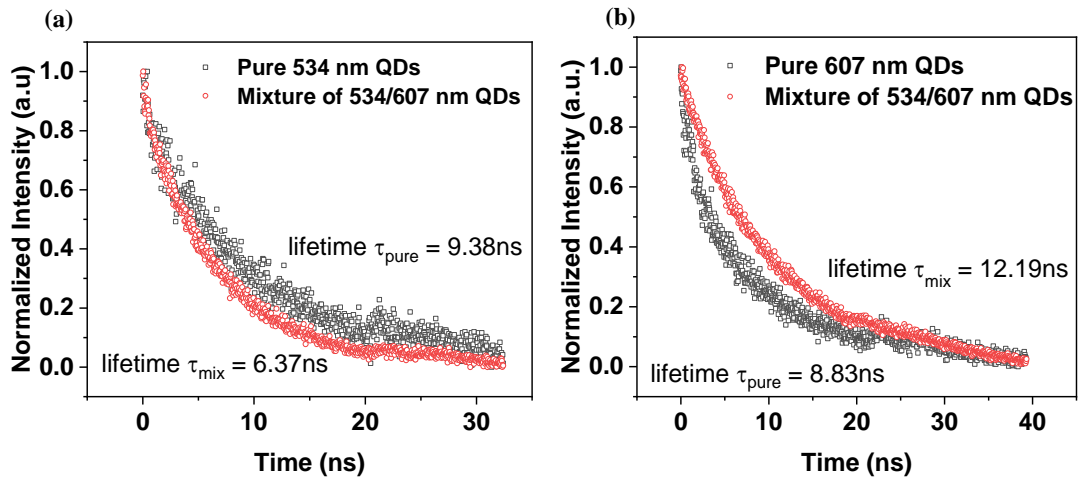


Figure 4.4 Time-resolved photoluminescence spectra of pure QDs and a 1:3 mixture of InP 534/607 nm QDs. (a) TRPL spectra of pure 534 nm QDs and mixed QDs, monitored at 534 nm. (b) TRPL spectra of pure 607 nm QDs and mixed QDs, monitored at 607 nm.

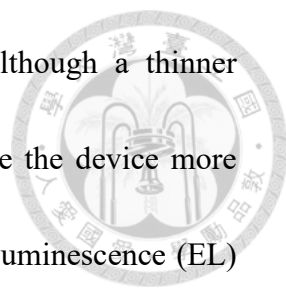
4.3 Performance of the quantum dot light-emitting diode



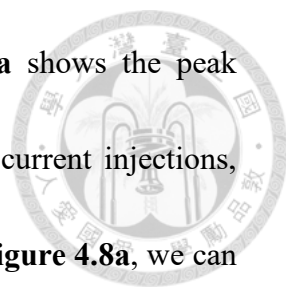
device

The energy level diagram of the layers used for the QD-LED layers is shown as **Figure 4.5**^[46-49]. The device is designed with a positive electrode at the ITO end and a negative electrode at the Ag end. ZnO, acting as the electric transport layer, possesses a low valence band and excellent hole-blocking capability. Once a voltage is applied to the device, holes attempting to flow from the active layer to ZnO are blocked, and thus confined within the active layer, as well as InP QDs layer. On the other hand, PVK serving as the hole transport layer, exhibits a high valence band. When a voltage is applied to the device, PVK can effectively prevent electrons from flowing through from the active layer, confining them within the active layer instead. As a result, efficient recombination of electrons and holes can occur in the active layer, generating a large number of photons. Additionally, 534 nm QDs have a larger bandgap energy compared to the 607 nm QDs. Therefore, carriers can readily transfer from the green QDs to the red QDs, enhancing the emission from the red QDs^[50-51].

Figure 4.6 shows the current-voltage (I-V) characteristic of the mixed InP device. The turn-on voltage is approximately 3.5 V when the thickness of the PEDOT:PSS layer is 60 nm. However, when the PEDOT:PSS layer thickness is varied to 25 nm and 85



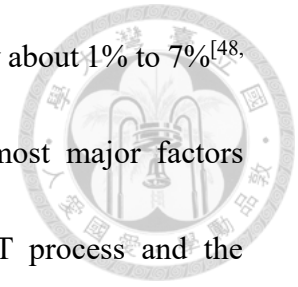
nm, the turn-on voltages are 1.8 V and 5.2 V, respectively. Although a thinner PEDOT:PSS layer can lower the turn-on voltage, it can also make the device more susceptible to decay. The inset displays a real photo of the electroluminescence (EL) image of the mixed InP device emitting light under an applied voltage of 5 V. The emission area is 2 mm×2 mm with uniform illumination. **Figure 4.7a** shows the EL spectra of the mixed InP device under applied current injection ranging from 5 mA to 25 mA, which corresponds to applied voltages ranging from 4.37 V to 9.26 V. The primary emission peak is observed at around 617 nm, with a full width at half-maximum (FWHM) of approximately 49 nm. Additionally, there is a smaller peak present around 545 nm, which is attributed to the emission contribution from the 534 nm QDs. Inset shows EL spectra with a focus on current levels of 5, 7.5, and 10 mA. In comparison to the EL spectrum obtained under large current injection, these three spectra exhibit a distinct peak within the green wavelength range. As the current increases, the peak around 545 nm becomes less prominent. This indicates that the energy transfer from the 534 nm to the 607 nm QDs intensifies as the current increases. When the mixed InP QD-LED device was driven by a voltage bias, the peak wavelength in the EL spectrum exhibited a slight red shift compared to PL, shifting from 609 nm to 617 nm, as clearly observed in **Figure 4.7b**. The red shift of EL peak may be attributed to either the electric-field-induced Stark effect or enhanced interdot interactions arising from the



reduced interdot distance in close-packed QDs^[52-54]. **Figure 4.8a** shows the peak intensities of the red and green spectra as a function of different current injections, based on the EL spectra in the **Figure 4.7a**. Through the result of **Figure 4.8a**, we can calculate the ratio between the red and green peak intensities as a function of different current injections, which is presented in the **Figure 4.8b**. The ratio increases as the current injection increases up to 15 mA, resulting in a shift of the color coordinates towards the red side. However, when the current exceeds 15 mA the ratio becomes saturated. And the intensity of the red peak is about 12 times greater than that of the green peak. When the mixed QDs were excited by 374 nm pulsed laser (1.73 mJ/cm²), the ratio of emitted red band to green band is about 3.9. The higher ratio of EL emission than PL means more energy transfer from the 534 nm QDs to the 607 nm QDs.

The luminous current efficiency and external quantum efficiency (EQE) of the device at various current injection levels are presented in **Figure 4.9**. The device achieved a maximum luminous current efficiency of 28.9 cd A⁻¹ and the highest EQE of 10.6% at a current injection level of 25.0 mA. **Table 4.1** provides a summary of the detailed device characteristics of recent reported red InP QD-LEDs. Our QD-LEDs demonstrate relatively good current efficiency compared to most published reports for red InP QD-based LEDs with similar structures, which typically exhibit efficiencies in the range of 2.5 to 25.2 cd A⁻¹. Additionally, the EQE of published red InP QD-LEDs

using a similar structure of PEDOT:PSS/PVK/QDs/ZnO is typically about 1% to 7%^[48, 55-56]. In comparison, our device exhibits a higher EQE. The most major factors responsible for the enhancement can be attributed to the FRET process and the reduction of reabsorption effect in the mixed QD-LEDs. It is because the light emission from the 607 nm QDs cannot be absorbed by the 534 nm QDs due to the smaller photon energy of red light than the bandgap of the 534 nm QDs. For the application of InP QDs in LED devices, only a small amount of research has been published. Despite this, InP QDs offer the advantages of low toxicity and wide spectral tunability. Combined with FRET and a simple LED device structure, mixed InP QD-LEDs are expected to be a priority choice for the next generation lighting technology.



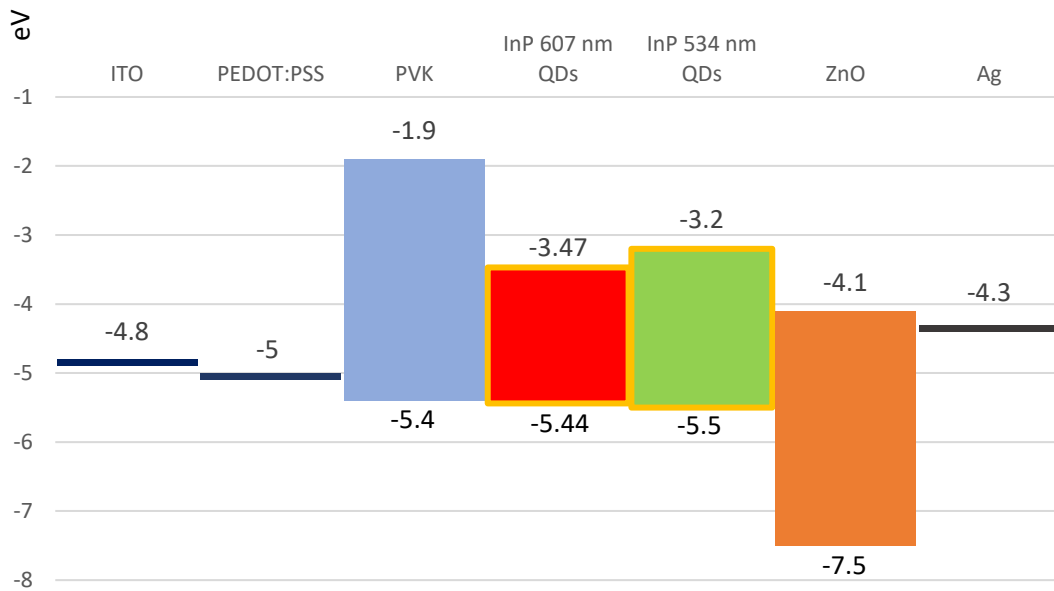


Figure 4.5 Schematic energy band diagram of the mixed InP QD-LED device.

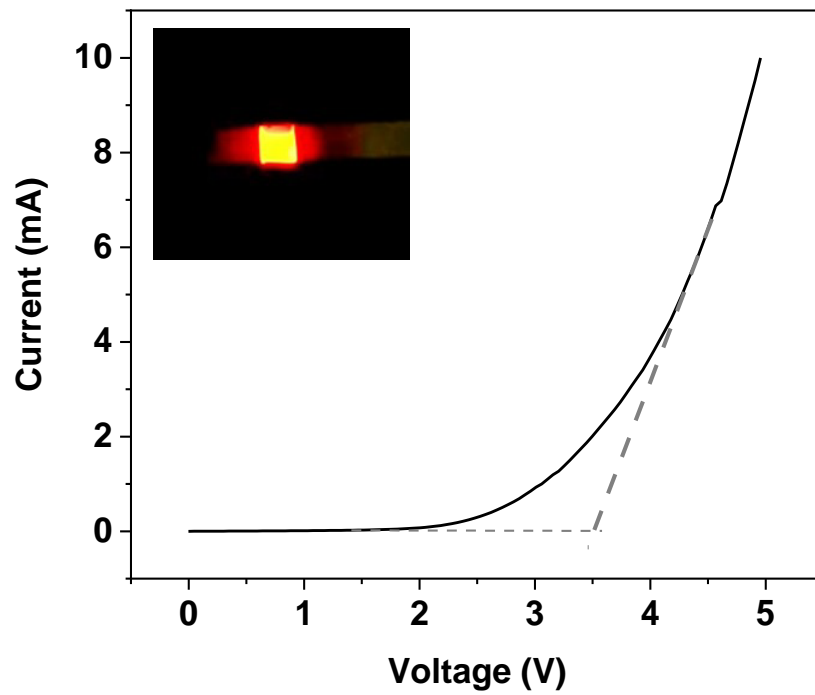


Figure 4.6 Current-voltage characteristic of the mixed InP device. The inset shows the real photo of the red-light emission from the mixed InP QD-LED device.

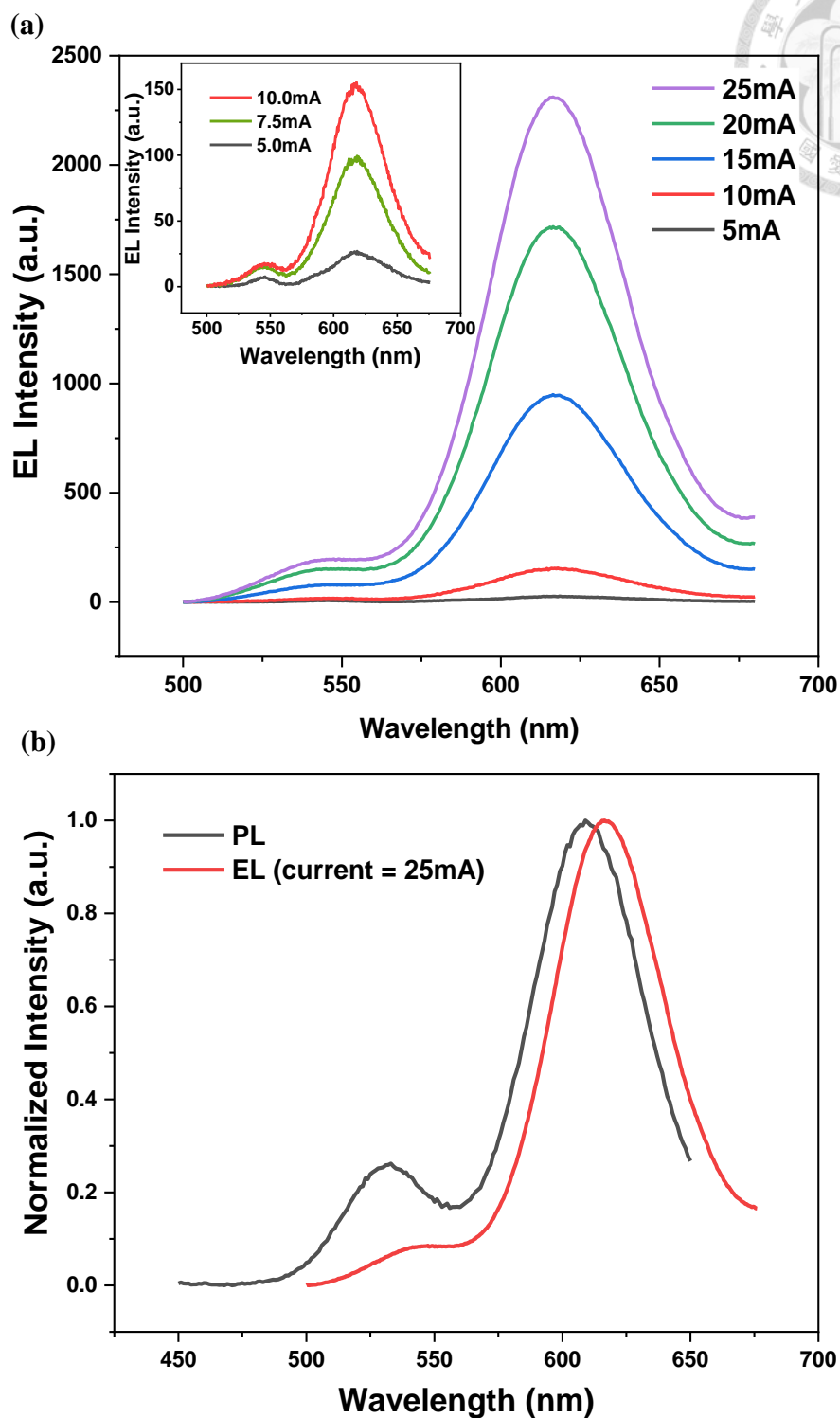


Figure 4.7 (a) EL spectra of the mixed InP QD-LED device at various levels of current injection. Inset is a zoomed-in EL spectra at current injection levels of 5.0, 7.5, and 10.0 mA. (b) A comparison between the PL spectrum of the QDs layer and the EL spectrum of the mixed InP QD-LED device under a current injection of 25 mA.

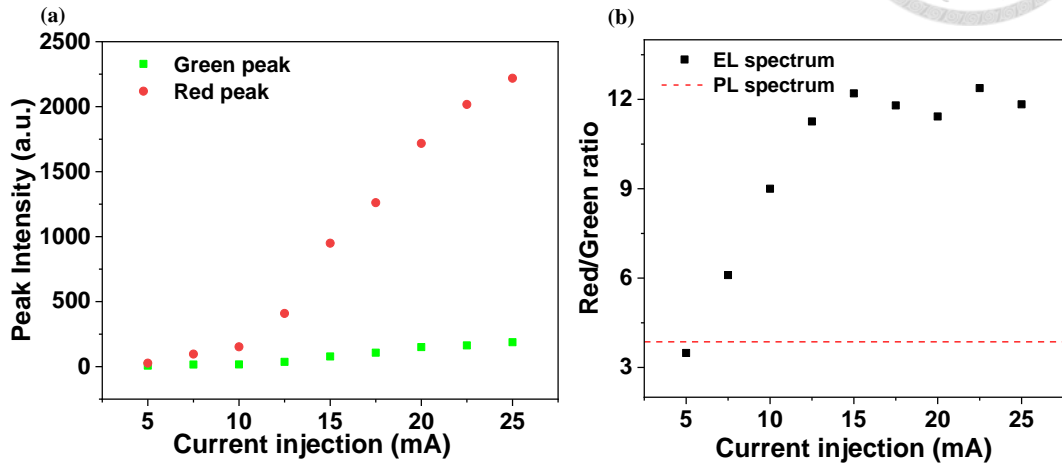


Figure 4.8 (a) Peak intensities of the red and green spectra as a function of different current injections (b) Ratio between the red and green peak intensities as a function of different current injections. The dashed line represents the ratio observed in the photoluminescence spectrum.

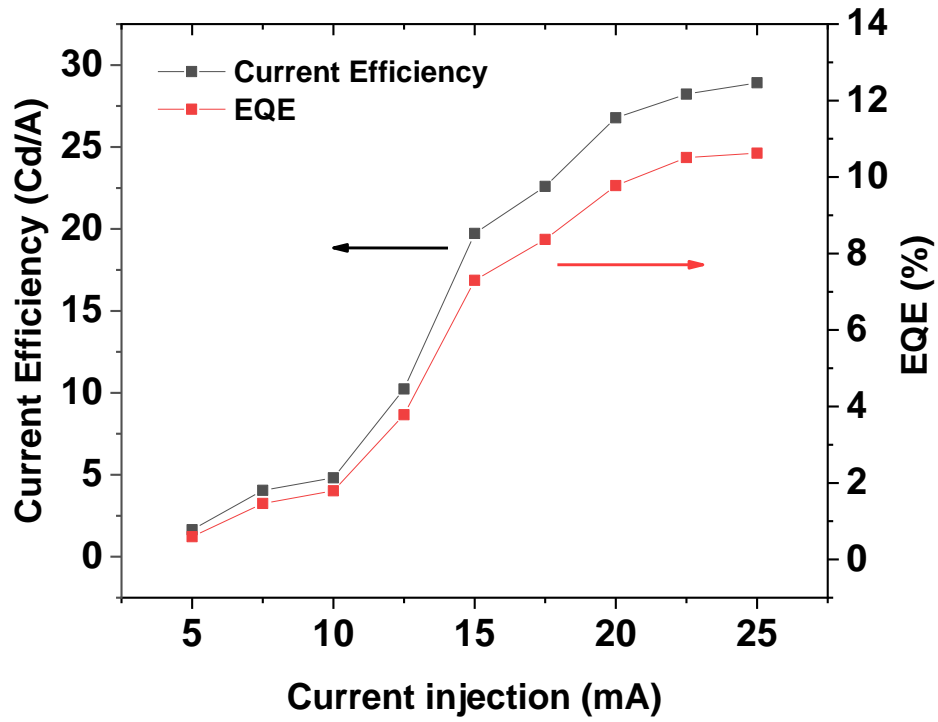
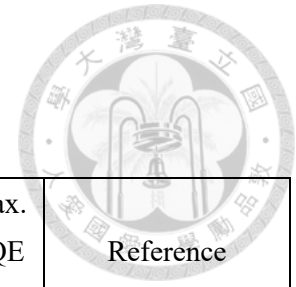


Figure 4.9 Luminous current efficiency and EQE of the mixed InP QD-LED device at different current injections.



Structure	Turn-on Voltage (V)	Current efficiency (cd A ⁻¹)	Max. EQE (%)	Reference
PEDOT:PSS/PVK/QD/ZnO/Ag	3.5	28.9	10.6	This work
PEDOT:PSS/PVK/QD/ZnO/Al	-	2.5	1.4	<i>Opt. Lett.</i> 2016 , <i>41</i> , 3984. ^[48]
PEDOT:PSS/TFB/QD/ZnO/Al	-	4.2	2.5	
PEDOT:PSS/Poly-TPD/ QD/Zn _{0.9} Mg _{0.1} O/Ag	1.8	14.7	12.2	<i>J. Am. Chem. Soc.</i> 2019 , <i>141</i> , 6448. ^[57]
PEDOT:PSS/TFB/QD/ Zn _{1-x} Mg _x O/Al	-	11.6	-	<i>ACS Appl. Mater. Interfaces</i> 2019 , <i>11</i> , 34067. ^[58]
PEDOT:PSS/TFB/QD/ZnMgO/Al	1.8-2.0	-	21.4	<i>Nature</i> 2019 , <i>575</i> , 634. ^[59]
PEDOT:PSS/PVK/QD/ZnO/Al	2.8	3.16	2.23	<i>Org. Electron.</i> 2021 , <i>96</i> , 106256. ^[55]
PEDOT:PSS/TFB/PVK/QD/ZnO/Al	2.4	4.13	2.87	
PEDOT:PSS/TFB/PVK/QD/ZnMgO/Al	2.8	5.46	4.05	
PEDOT:PSS/PVK/QD/ZnO/EGaIn	6.5	-	~7	<i>Mater. Chem. Phys.</i> 2022 , <i>287</i> , 126322. ^[56]
PEDOT:PSS/B-PTAA/QD/ZMO/Ag	2.0	25.3	20.4	<i>Nano Res.</i> 2023 , <i>16</i> , 7511. ^[60]

Table 4. 1 Performances of the previously reported red InP QD-LEDs.

Chapter 5

Conclusion




In our study, FRET mechanism was employed to tune the emission intensity and color of mixed InP QD-LED devices. By mixing 607 nm and 534 nm InP QDs with the best optimized ratio, we achieved an enhancement of the emission of the 607 nm wavelength with an energy transfer efficiency of 32%. Based on the unique features of the mixed QDs, we proposed an InP-based QD-LED utilizing FRET to increase its emission efficiency. Additionally, the reduction of reabsorption effect also plays an important role. The best performance achieved in our device possesses a current efficiency of up to 28.9 cd A^{-1} and EQE of 10.6%, which is better than pure QDs device without mixture and most published reports with similar structures. These results highlight the potential of eco-friendly InP QDs for use in light-emitting devices and open up new possibilities in the display field. The ability to achieve dominant color tuning, enhancement through FRET, and reduction of reabsorption effect is beneficial for the development of highly efficient light emitting devices. They can be widely used not only in the display industry but also in optical communication, expanding the potential applications of this technology.

Reference



- [1] M. Liu, N. Yazdani, M. Yarema, M. Jansen, V. Wood, E. H. Sargent, *Nat. Electron.* **2021**, 4, 548.
- [2] C. B. Murray, C. R. Kagan, M. G. Bawendi, *Annu. Rev. Mater. Sci.* **2000**, 30, 545.
- [3] F. Yuan, T. Yuan, L. Sui, Z. Wang, Z. Xi, Y. Li, X. Li, L. Fan, Z. a. Tan, A. Chen, *Nat. Commun.* **2018**, 9, 2249.
- [4] J. Song, J. Li, X. Li, L. Xu, Y. Dong, H. Zeng, *Adv. Mater.* **2015**, 27, 7162.
- [5] Z. Liu, C. H. Lin, B. R. Hyun, C.-W. Sher, Z. Lv, B. Luo, F. Jiang, T. Wu, C. H. Ho, H. C. Kuo, *Light Sci. Appl.* **2020**, 9, 83.
- [6] H. Zhang, S. Wang, X. Sun, S. Chen, *J. Phys. Chem. C* **2017**, 5, 817.
- [7] Z. Tan, F. Zhang, T. Zhu, J. Xu, A. Y. Wang, J. D. Dixon, L. Li, Q. Zhang, S. E. Mohny, J. Ruzyllo, *Nano Lett.* **2007**, 7, 3803.
- [8] Y. R. Park, J. H. Doh, K. Shin, Y. S. Seo, Y. S. Kim, S. Y. Kim, W. K. Choi, Y. J. Hong, *Org. Electron.* **2015**, 19, 131.
- [9] Y. Yang, Y. Zheng, W. Cao, A. Titov, J. Hyvonen, J. R. Manders, J. Xue, P. H. Holloway, L. Qian, *Nat. Photon.* **2015**, 9, 259.
- [10] X. Dai, Z. Zhang, Y. Jin, Y. Niu, H. Cao, X. Liang, L. Chen, J. Wang, X. Peng, *Nature* **2014**, 515, 96.
- [11] R. Toufanian, A. Piryatinski, A. H. Mahler, R. Iyer, J. A. Hollingsworth, A. M. Dennis, *Front. Chem.* **2018**, 6, 567.
- [12] X. Jiang, Z. Fan, L. Luo, L. Wang, *Micromachines* **2022**, 13, 709.
- [13] B. Chen, D. Li, F. Wang, *Small* **2020**, 16, 2002454.
- [14] Y. H. Won, O. Cho, T. Kim, D. Y. Chung, T. Kim, H. Chung, H. Jang, J. Lee, D. Kim, E. Jang, *Nature* **2019**, 575, 634.

- 
- [15] V. Brunetti, H. Chibli, R. Fiammengo, A. Galeone, M. A. Malvindi, G. Vecchio, R. Cingolani, J. L. Nadeau, P. P. Pompa, *Nanoscale* **2013**, 5, 307.
- [16] L. Li, Y. Chen, G. Xu, D. Liu, Z. Yang, T. Chen, X. Wang, W. Jiang, D. Xue, G. Lin, *Int. J. Nanomed.* **2020**, 1951.
- [17] D. H. Shin, R. Lampande, S. J. Kim, Y. H. Jung, J. H. Kwon, *Adv. Electron. Mater.* **2022**, 8, 2200256.
- [18] B. Zhang, Y. Luo, C. Mai, L. Mu, M. Li, J. Wang, W. Xu, J. Peng, *Nanomater.* **2021**, 11, 1246.
- [19] P. Kathirgamanathan, L. M. Bushby, M. Kumaravel, S. Ravichandran, S. Surendrakumar, *J. Inf. Technol.* **2015**, 11, 480.
- [20] A. R. Clapp, I. L. Medintz, H. Mattoussi, *ChemPhysChem* **2006**, 7, 47.
- [21] B. R. Gautam, R. Younts, J. Carpenter, H. Ade, K. Gundogdu, *J. Phys. Chem. A* **2018**, 122, 3764.
- [22] M. C. Dos Santos, W. R. Algar, I. L. Medintz, N. Hildebrandt, *TrAC, Trends Anal. Chem.* **2020**, 125, 115819.
- [23] T. Ha, T. Enderle, D. Ogletree, D. S. Chemla, P. R. Selvin, S. Weiss, *Proc. Natl. Acad. Sci.* **1996**, 93, 6264.
- [24] K. F. Wong, B. Bagchi, P. J. Rossky, *J. Phys. Chem. A* **2004**, 108, 5752.
- [25] I. L. Medintz, H. Mattoussi, *Phys. Chem. Chem. Phys.* **2009**, 11, 17.
- [26] A. Sarkar, S. C. Bhattacharya, *J. Lumin.* **2012**, 132, 2612.
- [27] H. Chen, H. L. Puhl, S. V. Koushik, S. S. Vogel, S. R. Ikeda, *Biophys. J.* **2006**, 91, L39.
- [28] R. B. Sekar, A. Periasamy, *J. Cell Biol.* **2003**, 160, 629.
- [29] T. L. Shen, H. W. Hu, W. J. Lin, Y. M. Liao, T. P. Chen, Y. K. Liao, T. Y. Lin, Y. F. Chen, *Sci. Adv.* **2020**, 6, eaba1705.
- [30] H. Cao, J. Y. Xu, Y. Ling, A. L. Burin, E. W. Seeling, X. Liu, R. P. Chang, *IEEE J.*

Sel. Top. Quantum Electron. **2003**, 9, 111.

[31] M. Skruzny, E. Pohl, M. Abella, *Biosensors* **2019**, 9, 122.

[32] M. Liu, J. Zhao, S. Zhou, Y. Gao, J. Hu, X. Liu, X. Ding, *Nanomater.* **2018**, 8, 450.

[33] J.-I. Shim, D.-S. Shin, *Nanophotonics* **2018**, 7, 1601.

[34] A. M. Alshehawy, D.-E. A. Mansour, M. Ghali, M. Lehtonen, M. M. Darwish, *Processes* **2021**, 9, 732.

[35] Q. Sun, J. Hou, C. Yang, Y. Li, Y. Yang, *Appl. Phys. Lett.* **2006**, 89, 153501.

[36] J. Liang, L. Ying, W. Yang, J. Peng, Y. Cao, *J. Phys. Chem. C* **2017**, 5, 5096.

[37] C. Liu, C. Xiao, W. Li, *J. Phys. Chem. C* **2021**, 9, 14093.

[38] Y. Sun, J. H. Seo, C. J. Takacs, J. Seifter, A. J. Heeger, *Adv. Mater.* **2011**, 23, 1679.

[39] C. L. Takanishi, E. A. Bykova, W. Cheng, J. Zheng, *Brain Res.* **2006**, 1091, 132.

[40] L. Ma, F. Yang, J. Zheng, *J. Mol. Struct.* **2014**, 1077, 87.

[41] C. Berney, G. Danuser, *Biophys. J.* **2003**, 84, 3992.

[42] M. Lard, S. H. Kim, S. Lin, P. Bhattacharya, P. C. Ke, M. H. Lamm, *Phys. Chem. Chem. Phys.* **2010**, 12, 9285.

[43] A. Pietraszewska-Bogiel, T. Gadella, *J. Microsc.* **2011**, 241, 111.

[44] S. V. Koushik, S. S. Vogel, *J. Biomed. Opt.* **2008**, 13, 031204.

[45] C. T. Shih, Y. C. Chao, J. L. Shen, Y. F. Chen, *Opt. Express* **2023**, 31, 12669.

[46] W. Gu, X. Liu, X. Pi, D. Xingliang, S. Zhao, L. Yao, D. Li, Y. Jin, M. Xu, D. Yang, G. Qin, *IEEE Photonics J.* **2017**, PP, 1.

[47] W. Jiang, B. Kim, H. Chae, *Opt. Lett.* **2020**, 45, 5800.

[48] J. H. Jo, J. H. Kim, K. H. Lee, C. Y. Han, E. P. Jang, Y. R. Do, H. Yang, *Opt. Lett.* **2016**, 41, 3984.

[49] H. H. Kim, S. Park, Y. Yi, D. I. Son, C. Park, D. K. Hwang, W. K. Choi, *Sci. Rep.* **2015**, 5, 8968.

[50] C. E. Rowland, J. B. Delehanty, C. L. Dwyer, I. L. Medintz, *Mater. Today* **2017**,



20, 131.

[51] K. F. Chou, A. M. Dennis, *Sens.* **2015**, 15, 13288.

[52] Z. Wu, P. Liu, W. Zhang, K. Wang, X. W. Sun, *ACS Energy Lett.* **2020**, 5, 1095.

[53] P. Ramasamy, K. J. Ko, J. W. Kang, J. S. Lee, *Chem. Mater.* **2018**, 30, 3643.

[54] H. H. Kim, S. Park, Y. Yi, D. I. Son, C. Park, D. K. Hwang, W. K. Choi, *Sci. Rep.* **2015**, 5, 1.

[55] X. Zhu, Y. Liu, H. Liu, X. Li, H. Ni, H. Tao, J. Zou, M. Xu, L. Wang, J. Peng, *Org. Electron.* **2021**, 96, 106256.

[56] S. R. Son, K. P. Yang, J. Park, J. H. Lee, K. Lee, *Mater. Chem. Phys.* **2022**, 287, 126322.

[57] Y. Li, X. Hou, X. Dai, Z. Yao, L. Lv, Y. Jin, X. Peng, *J. Am. Chem. Soc.* **2019**, 141, 6448.

[58] D. Li, B. Kristal, Y. Wang, J. Feng, Z. Lu, G. Yu, Z. Chen, Y. Li, X. Li, X. Xu, *ACS Appl. Mater. Interfaces* **2019**, 11, 34067.

[59] Y.-H. Won, O. Cho, T. Kim, D.-Y. Chung, T. Kim, H. Chung, H. Jang, J. Lee, D. Kim, E. Jang, *Nature* **2019**, 575, 634.

[60] W. Du, C. Cheng, J. Tian, *Nano Res.* **2023**, 16, 7511.

